A Numerical Study of the Thermally Driven Plain-to-Basin Wind over Idealized Basin Topographies

STEPHAN F. J. DE WEKKER,* SHIYUAN ZHONG, JEROME D. FAST, AND C. DAVID WHITEMAN

Pacific Northwest National Laboratory, Richland, Washington

(Manuscript received 12 May 1997, in final form 29 September 1997)

ABSTRACT

Numerical experiments have been carried out with a two-dimensional nonhydrostatic mesoscale model to investigate the diurnal temperature range in a basin and the thermally driven plain-to-basin winds. Under clear-sky conditions, the diurnal temperature range in a basin is larger than over the surrounding plains due to a combination of larger turbulent sensible heat fluxes over the sidewalls and a volume effect in which energy fluxes are distributed through the smaller basin atmosphere. Around sunset, a thermally driven plain-to-basin flow develops, transporting air from the plains into the basin. Characteristics of this plain-to-basin wind are described for idealized basins bounded by sinusoidal mountains and the circumstances under which such winds might or might not occur are considered. In contrast with a previous numerical study, it is found that the height of the mixed layer over the plains relative to the mountain height is not a critical factor governing the occurrence or nonoccurrence of a plain-to-basin wind. The critical factor is the horizontal temperature gradient above mountain height created by a larger daytime heating rate over the basin topography than over the plains. Subsidence and turbulent heat flux divergence play important roles in this heating above mountain height.

1. Introduction

Under conditions of weak synoptic forcing, a large-scale mountain–plain wind circulation (Kleinschmidt 1922; Burger and Ekhart 1937; Staley 1959; Tyson and Preston-Whyte 1972; Reiter and Tang 1984; Toth and Johnson 1985; Kurita et al. 1990; Kimura and Kuwagata 1993; Doran and Zhong 1994; Bossert and Cotton 1994; Bossert 1997) feeds low-level air into mountain ranges during daytime and out of mountain ranges during nighttime, with the upper branch of the circulation blowing counter to the low-level flows. Valley and slope wind systems can be considered as small-scale components of this larger-scale mountain–plain wind system. The mountain–plain wind system is produced by horizontal temperature gradients (e.g., Burger and Ekhart 1937) that develop between the air over the mountains and the air at the same level over the plains, with the mountainous terrain acting as an elevated heat source during daytime and an elevated heat sink during nighttime.

Plateaus and basins are common land forms in many parts of the world, influencing atmospheric motions that extend in scale from tens of kilometers to thousands of kilometers. Previous investigators of large-scale thermally driven wind systems in mountainous areas have given special names to the mountain–plain wind systems that feed plateaus and basins. The mountain–plain wind system over a plateau has been called a plain-to-plateau wind (Mannouji 1982). Similarly, a mountain–plain wind system carrying air from the plains over a mountain range into a basin has been called a plain-to-basin wind (Kimura and Kuwagata 1993).

Plain-to-plateau and plain-to-basin wind systems have a variety of practical implications for local weather and air pollution transport and diffusion. Both wind systems affect storm development by transporting moisture and producing convergence zones over high terrain. They play an important role in aviation, agriculture, and forest fire meteorology by producing layers with strong wind shear. The plain-to-basin wind can cause basin air quality to change drastically when either clean or polluted air is transported into a basin. The air quality in large cities that are situated in basinlike environments, such as Los Angeles and Mexico City, may be affected considerably by these winds. It is thus important to investigate the conditions under which the plain-to-basin wind occurs and the effects of basin topography on its characteristics.

Kimura and Kuwagata (1993) recently observed plain-to-basin winds in two Japanese basins and performed simulations with a two-dimensional hydrostatic

* Current affiliation: Atmospheric Science Programme, Department of Geography, University of British Columbia, Vancouver, British Columbia, Canada.

Corresponding author address: Stephan F. J. de Wekker, Atmospheric Science Programme, Department of Geography, University of British Columbia, Vancouver, BC V6T 1Z2, Canada.
E-mail: dewekker@geog.ubc.ca

mesoscale model for several basin topographies. They concluded that plain-to-basin winds do not occur when the mixed layer height over the plains is lower than the mountain height. In contrast, our results will show that the mixed layer over the plains does not necessarily have to grow above the mountain height to generate plain-to-basin winds.

Basin atmospheres experience a larger diurnal temperature range than the atmosphere over a nearby plain at the same elevation (Kondo et al. 1989). The large diurnal temperature range in basin (or valley) atmospheres has been primarily attributed to a volume effect in which energy fluxes into the basin atmosphere are distributed through a smaller volume than over the plain, amplifying the temperature change in the basin volume relative to the plain. This volume effect (which is a key tenet of mountain–valley flow theory) was first suggested by Wagner (1932, 1938) and was further investigated by Steinacker (1984) and McKee and O'Neal (1989). Our numerical study will show that the volume effect is not the only factor that explains the larger diurnal temperature range in the basin atmosphere than in the atmosphere over the plains.

In this study, a mesoscale model is employed to examine the diurnal temperature range in a basin and the thermally driven plain-to-basin wind for a variety of simulations with different basin geometries. Characteristics of the plain-to-basin wind, as well as factors that affect the development of the plain-to-basin wind, will be discussed.

The mesoscale model and the numerical experiments are described in section 2. In section 3, the diurnal temperature range in the basin is investigated. This is followed by a description of the general characteristics of the plain-to-basin wind and their dependency on basin geometry in section 4. In section 5, the role of daytime mixed-layer height and other factors on the occurrence of the plain-to-basin wind is examined. A discussion of some of the results and conclusions are given in sections 6 and 7, respectively.

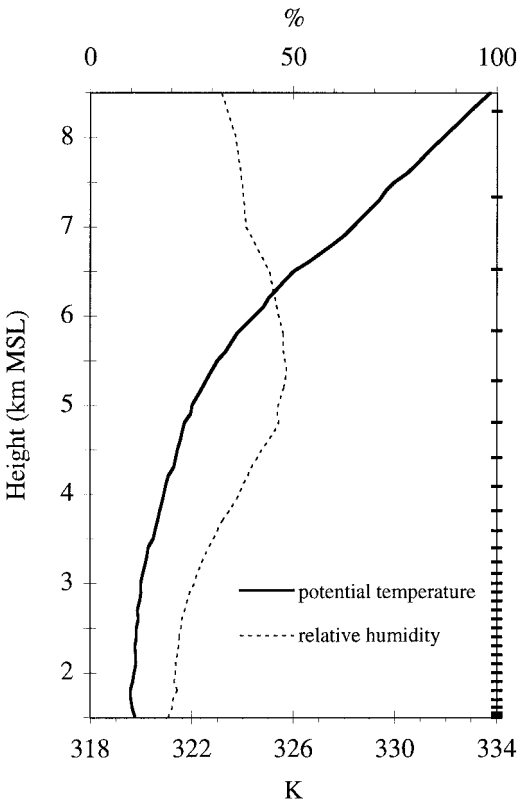

FIG. 1. July 1988 average 1700 LST potential temperature and relative humidity soundings for Grand Junction. Horizontal dashes on the right ordinate represent the vertical grid levels used in the simulations up to a height of 7 km AGL.

2. Numerical model

The Regional Atmospheric Modeling System (RAMS), as described by Pielke et al. (1992), is used in this study. The ability of RAMS to model complex terrain phenomena has been demonstrated by previous studies (Bossert and Cotton 1994; Doran and Zhong 1994; Jackson and Steyn 1994; Fast 1995; Fast et al. 1996; Bossert 1997; among others). The version of RAMS used in this study (version 3a) features a Mellor–Yamada level 2.5 turbulence closure scheme. Cumulus and microphysical parameterizations are not activated, so water vapor is treated as a passive scalar. The Mahrer and Pielke (1977) shortwave and the Chen and Cotton (1983) longwave parameterization schemes are used to determine the heating and cooling caused by radiative flux divergence. The calculation of the turbulent fluxes of sensible and latent heat in the surface layer is based on similarity equations (Louis 1979). Eleven soil levels are used, down to a depth of 1 m below the surface with a grid spacing varying from 5 cm near the surface to 15 cm at a depth of 1 m. RAMS employs a terrain-following coordinate system. The vertical resolution used in the simulations ranges from 25 m near the surface to 1000 m near the upper boundary and is depicted for the first 7000 m above ground level (AGL) on the right ordinate of Fig. 1. The upper boundary at 16 300 m consists of a rigid lid, and radiative lateral boundary conditions are employed following Klemp and Wilhelmson (1978a,b). A damping scheme is applied to the three vertical layers below the upper boundary in which the amplitudes of vertically propagating gravity waves are gradually suppressed to reduce wave reflection from the rigid lid. In the two-dimensional mode of RAMS there is no variation in the north–south direction, and the solution is computed for an east–west-oriented vertical plane.

The initial temperature and humidity fields are horizontally homogeneous and are based on a monthly average of 1700 local standard time (LST) soundings during July 1988 at a site in the Rocky Mountains [Grand Junction, 1524 m mean sea level (MSL)]. The corre-

TABLE 1. Summary of the model setup for the two-dimensional simulations.

Location	40°N, 105°W 1500 m MSL
Initialization	Temperature and humidity: Grand Junction mean sounding 1700 LST July 1988 Wind: westerly at 0.1 m s^{-1}
Simulation length	36 h
Time step	grid 1: 16 s grid 2: 8 s
Horizontal resolution	grid 1: 3000 m grid 2: 1000 m
Number of horizontal grid points	grid 1: 150 grid 2: 150–340
Fractional soil moisture content	0.25
Surface characteristics	Short grass on sandy loam Roughness length is 5 cm
Top boundary condition	Rigid lid
Lateral boundary condition	Klemp and Wilhelmson (1978a, b)
Coriolis force	Activated
Time differencing scheme	Leapfrog
Turbulent diffusion schemes	Horizontal diffusion: deformation scheme Vertical diffusion: Mellor–Yamada level 2.5 scheme
Radiation scheme	Shortwave radiation: Mahrer and Pielke (1977) Longwave radiation: Chen and Cotton (1983)

TABLE 2. Topographic parameter values for the primary simulations.

α	0, 0.25, 0.5, 0.75, 1
W_b	10, 20, 40, 80 km
H_m	0.5, 1, 2 km
W_m	20 km for a mountain height of 0.5 km 40 km for a mountain height of 1 km 80 km for a mountain height of 2 km Constant average slope angle $\approx$ 2.9°

sponding vertical potential temperature and relative humidity profiles are shown in Fig. 1. This temperature and humidity structure is assumed to be typical for afternoon summertime conditions. It should be recognized, however, that temperature inversions that are present at different heights on individual days will be averaged out in this procedure. The height of the plains in the model domain is 1500 m MSL, based on Grand Junction's altitude. Initial winds are assumed to be 0.1 m s^{-1} and westerly everywhere. Soil and vegetation properties are also assumed to be invariant. The initial soil moisture fraction is set to 0.25. Boundary layer development is very sensitive to the chosen soil moisture fraction as it affects the partitioning of the available energy at the earth's surface into turbulent latent and sensible heat fluxes. The value 0.25, a relatively dry value, was chosen so that the modeled vertical potential temperature profile over the plains 24 h after initialization would be similar to the initial profile. Local sunrise occurs around 0600 LST, while sunset occurs at about 1900 LST. A summary of the model setup is given in Table 1.

Idealized basin topography was used for the simulations to isolate the effects of dominant terrain features and provide insight into the physical mechanisms that affect the circulation systems. Basin floors were horizontal and bounded by uniform sinusoidally shaped mountains. Sixty two-dimensional simulations were carried out in which mountain height H_m, mountain width W_m, basin floor height H_b, and basin width W_b, were varied. These topographic parameters are defined in Fig. 2 and the values used are given in Table 2. Variations in mountain topography were specified so that slope angles were conserved, that is, doubling the mountain height required a doubling of mountain width. Of the 60 simulations, 12 had the basin floor height equal to the height of the surrounding plain, H_p (1500 m MSL); 12 had a plateau with a height equal to $H_p + H_m$ (2000, 2500, or 3500 m MSL), and the remaining 36 simulations had basin floors at intermediate heights [at H_p + (0.25, 0.5, and 0.75)H_m]. Additional simulations were carried out to investigate the effects of mixed-layer height, ambient wind, initialization time, and other effects. Because of the large number of simulations with different combinations of topographic parameters, only two-dimensional simulations were performed.

To minimize boundary effects, lateral boundaries were set at least 50 km away from the basin topography and the simulations were carried out with a nested grid configuration where the nested grid included the basin and the mountain ridges. The size of the domain in the outer grid, where the grid spacing was 3 km, was kept constant in all runs at 450 km. The domain in the inner grid, with a grid interval of 1 km, varied from 150 to

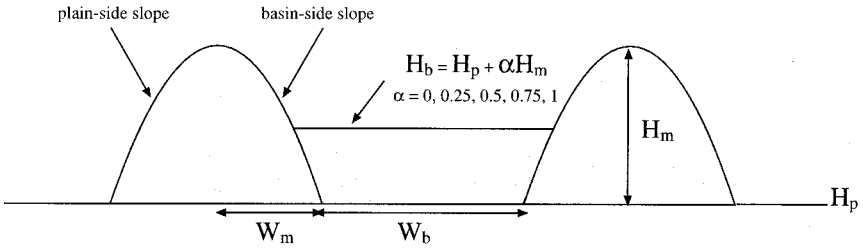

FIG. 2. Definition of the parameters H_m, H_b, H_p, W_b, and W_m used to describe terrain geometry and location of the plainside and basinside slopes.

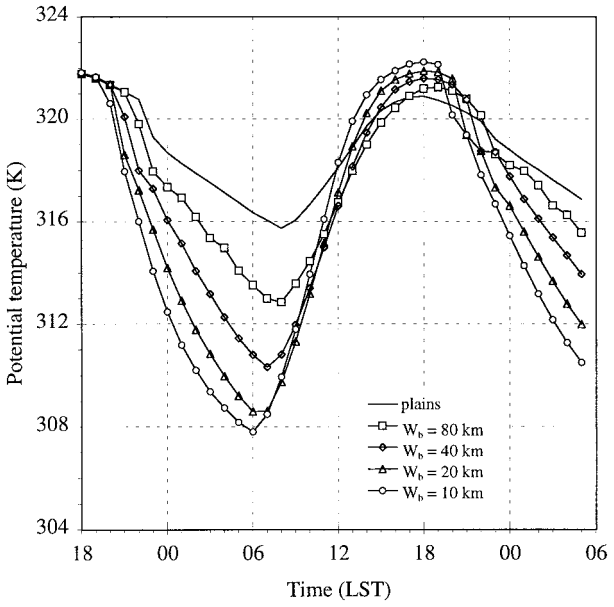

FIG. 3. Diurnal temperature ranges averaged up to 2500 m MSL for the plains and for basin topographies with $H_m = 1$ km; $\alpha = 0$; and $W_b = 10$, 20, 40, and 80 km.

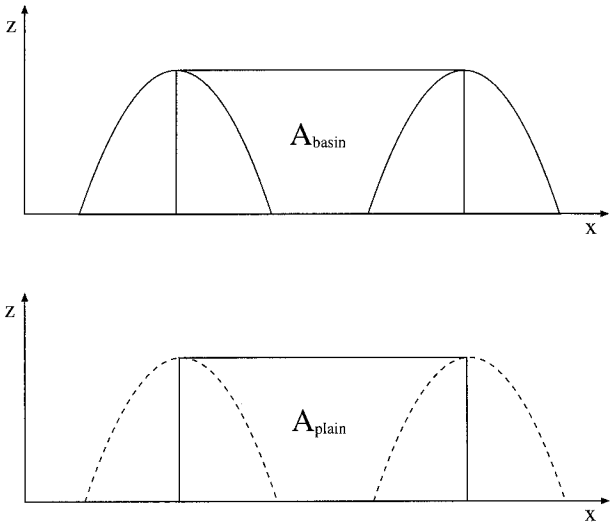

FIG. 4. Illustration of the TAF concept. For this idealized basin topography, TAF is simply the ratio of the areas of the shaded cross sections over the plains (A_{plain}) and the basin (A_{basin}).

340 km, depending on the horizontal extent of the particular basin topography.

3. Diurnal temperature range in the basin

An important factor for the development of a thermally driven wind system over basin topography is the difference in diurnal temperature range in the basin atmosphere compared to that over the plains atmosphere. The diurnal temperature ranges for the basins with $H_m = 1$ km and $\alpha = 0$ are shown in Fig. 3 for different basin floor widths. The values shown were obtained by averaging a vertical column of grid points up to H_m (where H_m equals 1 km AGL) over the basin center. Averaging the potential temperature values vertically up to H_m or averaging over the whole basin area up to H_m did not make a significant difference. For comparison, the diurnal temperature range for an air column over the plains (located immediately at the foot of the mountain base), vertically averaged up to H_m, is also shown in Fig. 3. It is evident that the heating and cooling rate within the basin is larger than over the plains, with an increase in the diurnal temperature range as the basin floor width decreases. Interestingly, the larger diurnal temperature range in basins is attained primarily by colder nighttime rather than by warmer daytime temperatures compared to those over the plains. Differences in maximum temperatures between the basin and the plains are only about 2 K, while differences in minimum temperature can be up to 8 K. Advective cooling plays an important role for the generation of these low temperatures in basins during nighttime, as was shown, for example, in a numerical study by Fast et al. (1996). The sudden decrease in temperature after 1900 LST in the basin atmosphere is related to the development of a plain-to-basin wind around that time, as will be shown in section 4.

It is usually argued that the larger diurnal temperature range in basins and valleys is primarily due to a volume effect (Steinacker 1984; Whiteman 1990). From combining the first law of thermodynamics and Poisson's equation, the potential temperature change $d\theta$ (K) in an air volume V (m^3) with density ρ (kg m^{-3}) and specific heat c_v (J kg^{-1} K^{-1}) for a given heat input dq (J) is simply given by

$$dq = \rho V c_p (T/\theta)\, d\theta, \tag{1}$$

where $(T/\theta) \approx 1$ is the ratio of actual temperature to potential temperature. An energy increment coming into or out of the top of the basin will heat or cool the basin atmosphere. A similar increment coming into or out of the plains atmosphere will heat or cool a larger atmospheric volume, therefore producing a smaller temperature change. The volume effect has been described in terms of a topographic amplification factor or TAF (Whiteman 1990), which is illustrated in Fig. 4 for idealized basin and plains cross sections. The TAF, defined as the ratio of the temperature change in an enclosed basin volume to that in an enclosed equal-width plains volume for an equal heat input, is simply the ratio of the volumes $\text{TAF} = d\theta_{basin}/d\theta_{plain} = V_{plain}/V_{basin}$, or $\text{TAF} = A_{plain}/A_{basin}$ for the two-dimensional example in Fig. 4. TAF values for the various basin geometries used in this study ranged from 1.065 to 2.304.

The basin–plain diurnal temperature range ratio $\Delta\theta_{basin}/\Delta\theta_{plain}$ as a function of TAF for three different mountain heights is shown in Fig. 5. Based on the definition of TAF, the relationship between these two variables would be a straight 1:1 line if the total sensible

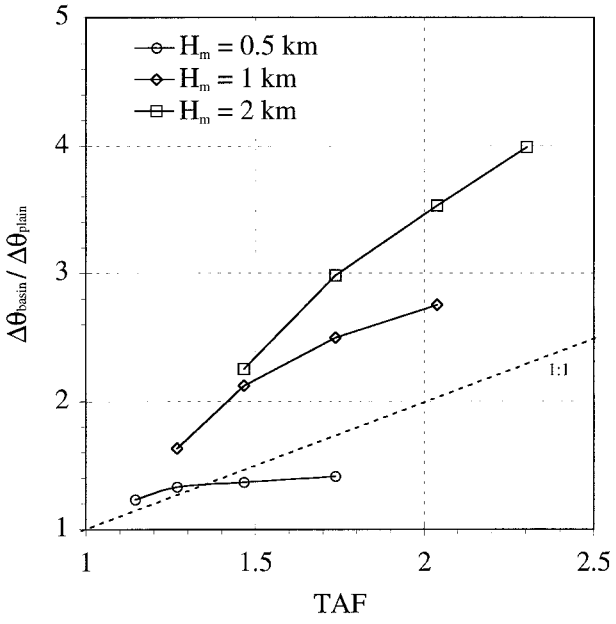

FIG. 5. Diurnal potential temperature range in the basin atmosphere relative to that over the plains atmosphere (vertically averaged up to H_m) as a function of TAF for the simulations with $\alpha = 0$. The 1:1 line depicts the relationship if only the volume effect is taken into consideration.

heat gain and loss were the same for the basin and the plain atmospheres and if the basin and plain atmospheres were enclosed by a rigid lid at ridge top height. In that case, all the sensible heat from the basin floor and sidewalls would be used to heat or cool the entire atmosphere below ridge height and no heat would be transported out of or into the enclosed basin volume. Figure 5 shows that there is an increase of the basin–plain diurnal temperature range ratio with TAF, but a 1:1 relationship is not evident. There is a clear dependency of the relationship on mountain height and, except for $H_m = 0.5$ km, the ratio is always larger than would be expected from consideration of the volume effect alone. The explanation for the larger basin–plain diurnal temperature range ratios is found in total sensible heat input differences between the basin and the plains. Despite invariant surface properties at the lower model boundary, modeled turbulent heat fluxes are inhomogeneous, with much larger values over the sloping sidewalls than over the flat terrain. The total sensible heat gain and loss for the basin atmosphere is therefore much larger than in an equivalent plains atmosphere. Accordingly, the ratios of the diurnal temperature ranges are generally much larger than predicted by the volume effect alone. The turbulent heat fluxes in the model are calculated with the scheme of Louis (1979) in which the fluxes are proportional to the wind speed. Therefore, the slope flows are likely to be responsible for the larger turbulent sensible heat fluxes over the slopes in the model.

Interestingly, Steinacker (1984) shows from observations that, on average, the calculated volume effect for the Austrian Inn valley accounts for the observed differences in vertically averaged diurnal temperature ranges between a valley site and an adjacent plain site and implies that the volume effect is the main reason for the larger diurnal temperature range in valleys than over the plains. He also notes that on individual days, the ratio of the diurnal temperature ranges might be larger due to larger sensible heat fluxes over the valley sidewalls caused by differences in surface properties. The numerical model produces larger sensible heat fluxes over the sidewalls even with homogeneous surface properties.

The volume effect was first suggested by Wagner (1932) as one of several factors that might explain the larger diurnal temperature ranges in valleys than over the plains. Wagner argues further that another factor might be the larger vertical turbulent heat exchange in the valleys than over the plains. Not much attention has been given to this factor since his early publication, but it appears to play a role in the simulated heat budget of a basin.

Figure 5 shows that for a particular value of TAF, the ratio is generally larger for higher mountains (i.e., deeper basins). Higher mountains have longer slopes (since the slope angle was kept constant in all our simulations) that, particularly during nighttime, produce stronger slope winds and therefore enhance the vertical turbulent heat exchange. Another factor that contributes to the mountain height dependency is the height of the mixed layer in the basin relative to the mountain height. For lower mountains, the simulated mixed layer in the basin generally grows above the mountain height in the afternoon. In these cases, the sensible heat from the basin floor and sidewalls is not used entirely for heating the atmosphere within the basin but also for heating an atmospheric volume above the mountain height. Obviously, TAF does not take this into account. In the case of higher mountains, on the other hand, mixed-layer heights stay lower relative to mountain height and more of the energy from the basin floor and sidewalls is confined within the basin below the mountain height. Evidence that this factor is playing a role is given by the fact that for $H_m = 0.5$ km, there are cases where the ratio of the basin—plain diurnal temperature range is smaller than predicted by the volume effect alone (see Fig. 5). The mixed-layer height in the basin obviously regulates the volume in the basin that is being heated and consequently affects the relationship between TAF and the heating rate. A similar effect was also noted by Steinacker (1984). On days with deep convection, thermally driven upvalley flows are less pronounced, implying that temperature differences between the valley and the plains are relatively small. Steinacker also notes that on an average winter day, larger differences in vertically averaged diurnal temperature ranges are observed between a site in the Austrian Inn valley and a site on the adjacent plain than in summertime due to the larger

static stability of the valley atmosphere on an average winter day.

Finally, it can be seen in Fig. 5 that for a given mountain height the rate of increase in the ratio of the diurnal temperature range in the basin to that over the plains decreases with increasing TAF (or similarly, decreasing basin width or basin volume in these particular cases). A possible reason for this might be a decrease in the total sensible heat gain and loss due to, for example, a different behavior of slope winds in basins with a larger TAF. Also, relatively more energy may be used to heat the atmosphere above mountain height than below mountain height as the basin volume decreases.

The difference in temperature above mountain height between the basin and the plains atmosphere is affected to a certain degree by the relative heating inside the basin and over the plains. As will be shown in section 5, it is this horizontal temperature gradient above the mountain height that affects the occurrence of the plain-to-basin wind.

4. Thermally driven wind systems over basin topography

a. General characteristics

To describe the general characteristics of thermally driven wind systems over idealized basin topography, the discussion will first be directed to a simulation using a basin that is 1 km deep with a 20-km-wide basin floor. Differences between this reference simulation and simulations where other basin geometries were used will be discussed subsequently.

The simulated u component of the wind and the potential temperature fields at 1000, 1800, and 2000 LST (i.e., 17, 25, and 27 h after model initialization) for the reference basin topography are shown in Fig. 6. At 1000 LST, upslope winds have developed in an approximately 300-m-thick convective boundary layer over the plainside and basinside slopes (Figs. 6a and 6d). Interestingly, the convergence of these upslope winds (denoted by arrows in Fig. 6) occurs not over the mountaintop, but over the plainside slope. Downslope flows are stronger on the plainside slope than over the basinside slope during most of the night, so that the transition from a downslope-directed flow to an upslope-directed flow takes longer on the plainside slope.

During daytime, a hydrostatically established pressure gradient produced by a large-scale horizontal temperature gradient between the elevated terrain and the plains forces the flow within the convective boundary layer over the plains to be directed toward the mountains. This plain-to-mountain wind generates a relatively large and deep upslope wind on the plainside slope as time proceeds. Before sunset at 1800 LST, the plain-to-mountain wind has grown to 1500 m AGL, approximately corresponding to the vertical extent of the convective boundary layer, and a well-developed return flow is present aloft (Figs. 6b and 6e). The convergence zone is located on the basinside slope at this time.

At 2000 LST (i.e., just after sunset), a shallow downslope wind layer has developed on the plainside slope. On the basinside slope, a plain-to-basin wind with a maximum magnitude of about 5 m s^{-1} occurs over the entire slope all the way down to the basin floor (Fig. 6c). Because of the relatively large magnitude of these winds, the downward turbulent heat fluxes along the basinside slopes are enhanced and temperatures start to cool rapidly. The sudden drop in basin temperatures after sunset, as was seen in Fig. 3, is thus associated with the onset of the plain-to-basin wind.

The diurnal course of the upslope component of the wind near the surface at a midslope point on both the plain- and basinside slopes for the same basin topography as in Fig. 6 is depicted in Fig. 7. The midslope point is defined here as the vertical grid point where the height is nearest to $H_b + [(H_p + H_m) - H_b]/2$ (see Fig. 2). Figure 7 clearly shows the asymmetric development of the thermally driven flow on the plain- and basinside slopes. The wind turns to an upslope direction about 2 h earlier on the basinside slope (between 0600 and 0700 LST) than on the plainside slope. This also explains why the upslope winds converge initially on the plainside slope, as was seen in Fig. 6a. The earlier onset is not affected by the slope orientation since the upslope wind also started earlier over the basinside slope of the eastern mountain ridge (not shown).

Figure 7 further shows that upslope winds on the plainside slope are generally stronger than those on the basinside slope, reaching a maximum speed of 7 m s^{-1} at 1400 LST. At 2100 LST, the plain-to-basin wind reaches its maximum with a speed of 7 m s^{-1}. The stronger cooling rate in the basin after sunset causes the temperature gradient between the basin and plains atmosphere that developed during the day to diminish quickly. Consequently, the speed of the plain-to-basin wind decreases significantly after 2100 LST reaching about 2 m s^{-1} at midnight. On the plainside slope, the change from an upslope to a downslope flow occurs 1 h later than on the basinside slope and the wind speed increases more gradually, reaching a steady 5 m s^{-1} after 0300 LST. The lower magnitude of the downslope directed flow on the basinside slope after midnight is partly due to the larger static stability of the nocturnal basin atmosphere. Furthermore, the slope winds at the plainside slope are intensified by a larger-scale mountain-to-plain wind.

b. Effects of basin geometry

The characteristics of the primary simulations were very similar. A plain-to-basin wind developed in almost all simulations except for some of the simulations with the widest basins. Therefore, the differences in the onset time, strength, and timing of the plain-to-basin wind as a function of basin width, mountain height, and basin

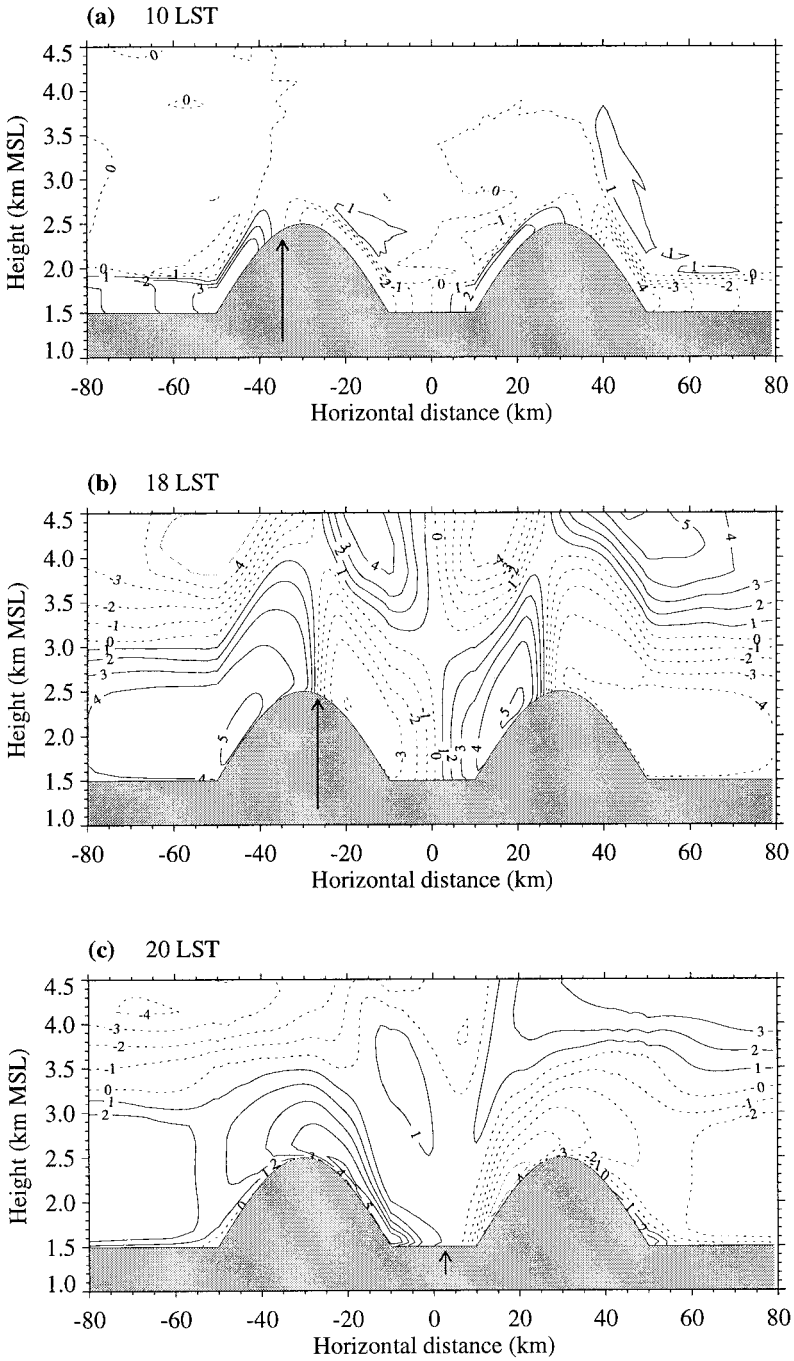

FIG. 6. The u component of the wind (m s^{-1}) at (a) 1000, (b) 1800, and (c) 2000 LST and potential temperature (K) at (d) 1000, (e) 1800, and (f) 2000 LST for a basin topography with $H_m = 1$ km, $W_b = 20$ km, and $\alpha = 0$. The arrows indicate the approximate position of a convergence zone.

elevation will now be discussed by selecting only subsets of the primary simulations.

Figures 8a–c show the effects of basin width, mountain height, and basin floor elevation on the wind speed at a midslope point on the basinside slope. The plain-to-basin wind maximum tends to occur earlier for narrower basins (Fig. 8a), but its timing is not significantly affected by mountain height (Fig. 8b) and for basins with elevated floors (Fig. 8c).

The maximum magnitude of the plain-to-basin wind increases for narrower basins (Fig. 8a) and higher mountains (Fig. 8b) but is not affected by basin floor elevation

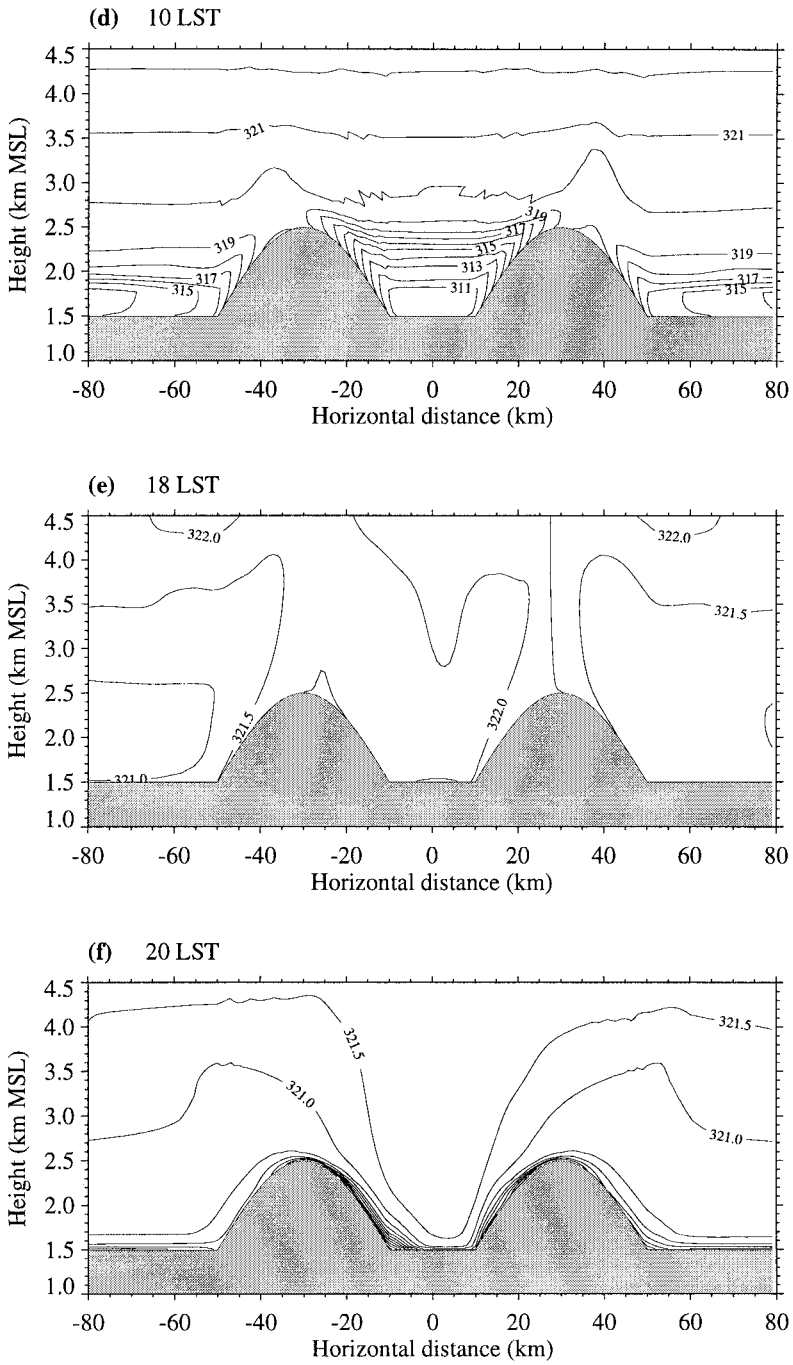

FIG. 6. (*Continued*)

(Fig. 8c). The increase in the downslope wind maximum with mountain height is mainly caused by an increase with mountain height of the locally generated downslope flows, as might also be inferred from the larger steady downslope wind speeds for higher mountains after 0000 LST. The onset time of the plain-to-basin wind is determined primarily by the cessation time of upslope winds on the basinside slope. Since upslope flows cease shortly after the surface sensible heat flux changes sign, the plain-to-basin wind almost always penetrates into the basin around sunset with a maximum variability of only about 2 h among the different basin topographies. Plain-to-basin winds tend to start somewhat later for simulations with wider basins (Fig. 8a), higher mountains (Fig. 8b), and less elevated basins (Fig. 8c). The earlier onset of the plain-to-basin wind for more elevated basins is partly due to the location of the midslope point, which is higher on the basinside slope for more elevated basin floors.

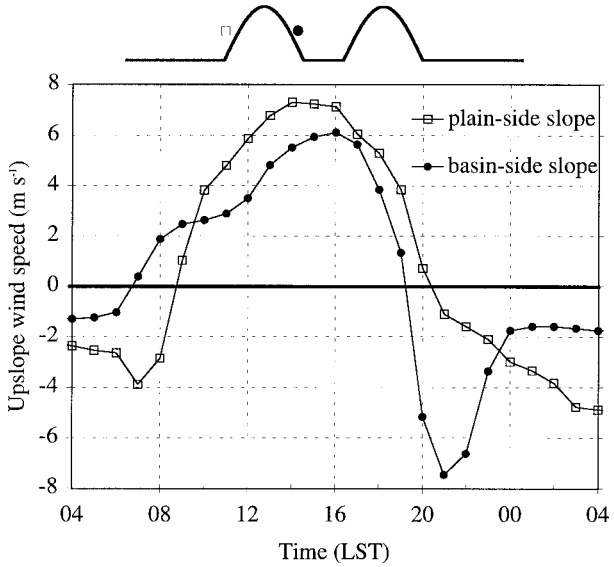

FIG. 7. Diurnal variation of the upslope wind component at a basinside and a plainside midslope point at about 100 m AGL for the same basin topography as in Fig. 6. The figure at the top of the plot shows a cross section of the basin topography, indicating the locations inside and outside the basin where the simulated wind data were taken.

Similar characteristics of the plain-to-basin wind as a function of basin width were found by Kimura and Kuwagata (1993), but they found a decrease of the downslope wind maximum with mountain height for mountains higher than 1 km (cf. their Figs. 5 and 6). It should be noted, however, that in their idealized basin topographies, the slope angle increases with increasing mountain height. This effect should also be taken into account in their results. The slope angles in our study are conserved between the different basin topographies. Other possible reasons for the discrepancy between their results and ours will become clear in the following sections.

The similarity in the spatial characteristics of the thermally driven wind systems as a function of basin floor height is demonstrated in Figs. 9a–c, which show the horizontal wind field at 2000 LST for $\alpha = 0$, 0.5, and 1, respectively. The plain-to-basin wind speed or, in the case of a plateau, the plain-to-plateau wind (Fig. 9c), does not change significantly as the height of the basin floor increases. Figures 9a–c further indicate that the basin floor height did not affect the characteristics of the upslope wind over the plainside slope. In general, the characteristics of the slope winds on the plainside slope were very similar for all basin geometries, thus independent of mountain height, basin width, and basin floor elevation.

5. Plain-to-basin wind and mixed-layer heights

Now that the general characteristics of the plain-to-basin wind and some differences due to basin topog-

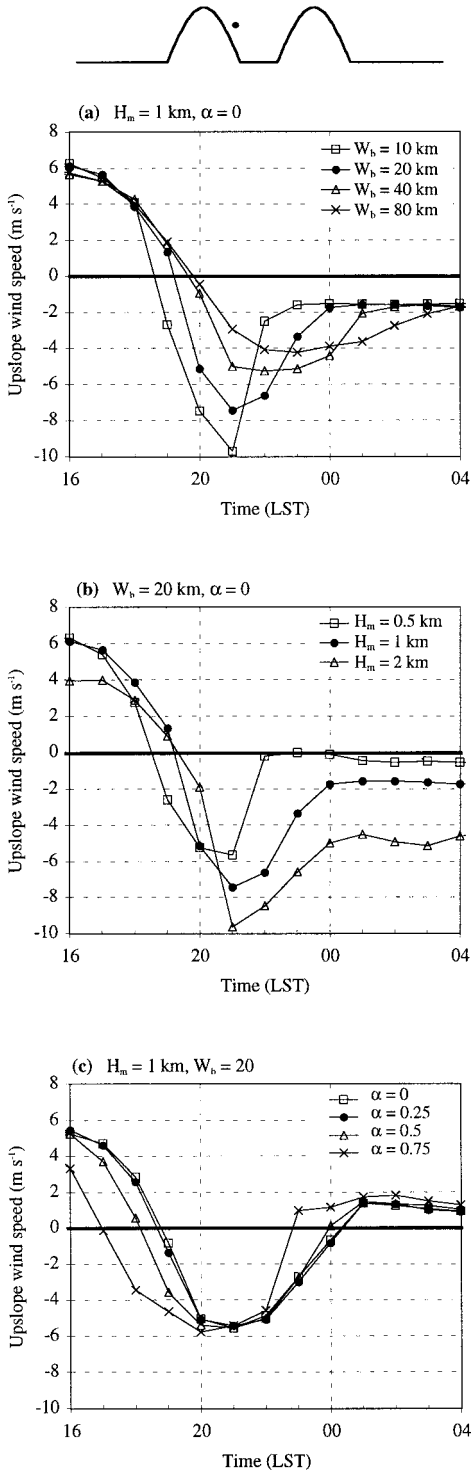

FIG. 8. Diurnal variation of the upslope wind component at a basinside midslope point at about 100 m AGL as a function of (a) basin width, (b) mountain height, and (c) basin floor elevation. The figure at the top of the plot shows a cross section of the basin topography, indicating the location where the wind data were taken.

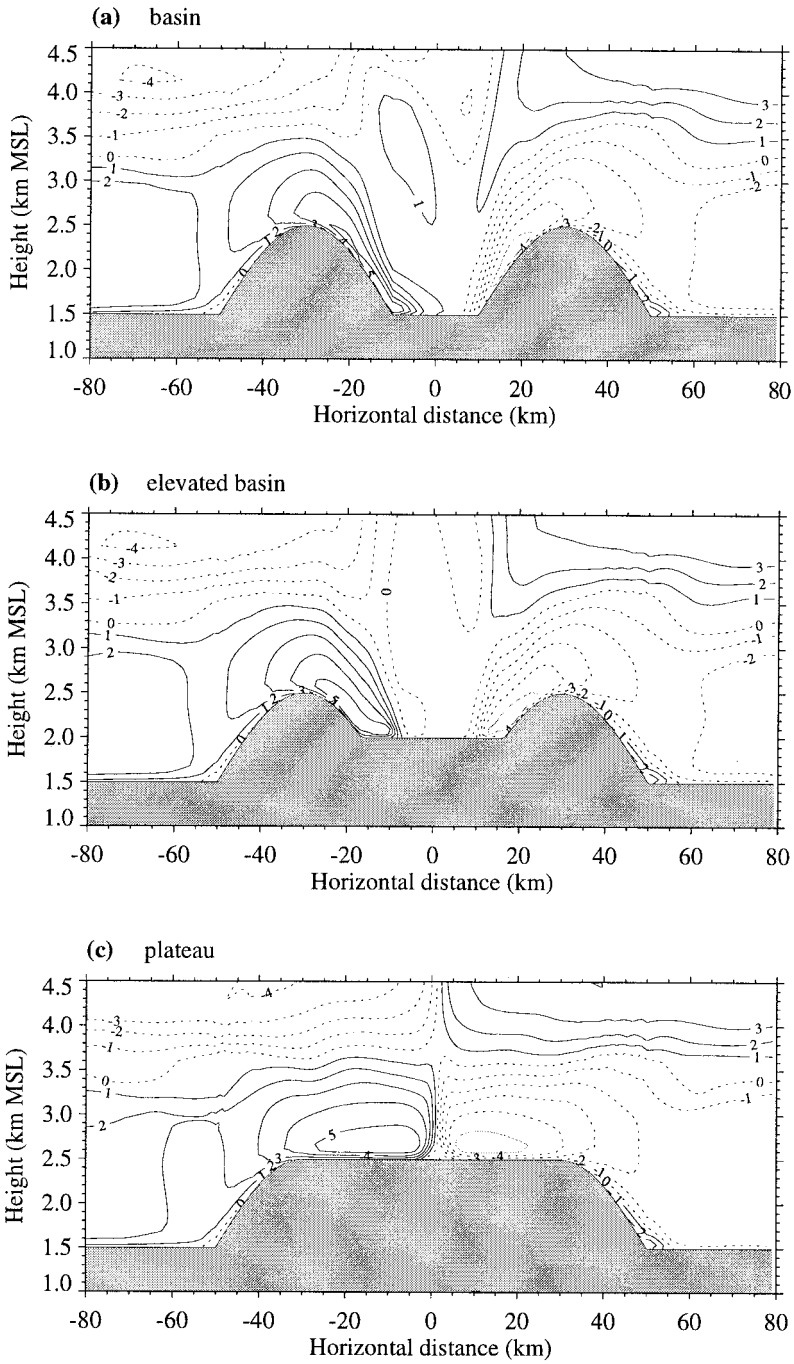

FIG. 9. The u component of the wind (m s^{-1}) in a basin topography with $H_m = 1$ km, $W_b = 20$ km and (a) $\alpha = 0$, (b) $\alpha = 0.5$, and (c) $\alpha = 1$ at 2000 LST.

raphy have been described, the next step is to determine the main factors that affect the development of the plain-to-basin wind. Knowledge of these factors will enable us to assess the probability that a plain-to-basin wind will occur, given the atmospheric conditions and the basin topography. Kimura and Kuwagata (1993) concluded that the mixed-layer height over the plains relative to mountain height is a critical factor. They inferred from their simulations that the plain-to-basin wind is generated only when the height of the mixed layer over the plains equals or exceeds mountain height.

To further investigate the relationship between mixed-layer heights and the plain-to-basin wind, we determined mixed-layer heights in all simulations by analyzing vertical profiles of potential temperature. The mixed-layer height was taken as the height where the

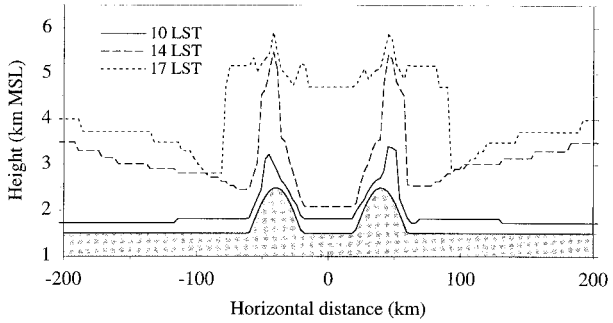

FIG. 10. Spatial variation of the mixed-layer height at 1000, 1400, and 1700 LST for a basin with $H_m = 1$ km, $W_b = 20$ km, and $\alpha = 0$.

vertical temperature gradient first becomes larger than 0.001 K m^{-1}. An example of the spatial behavior of mixed-layer height over the basin topography is shown in Fig. 10 for 1000, 1400, and 1700 LST. The model produces mixed-layer heights that generally follow the underlying terrain. In the regions over the plains close to the mountains and in the basin, initial mixed-layer growth is significantly reduced by sinking motions. The sinking motions compensate the rising motions, initiated by the upslope flows, over the mountain ridges where the mixed-layers heights are relatively large. Suppression of mixed-layer growth in basins and valleys has been observed by Kondo et al. (1989). In the basin atmosphere, the strong inversion that develops during the night also contributes to a slower growth rate of the daytime mixed layer. Mannstein (1988) has also suggested that a turbulent sensible heat flux gradient along sloping terrain with higher values higher up the slope tends to maintain a stable stratification. This could be a further reason for the relatively slow initial mixed-layer growth. By 1700 LST, the mixed-layer height in the basin increased considerably because of the strong heating in the basin and the final breakup of the temperature inversion. The spatial and temporal evolution of mixed-layer heights shown in Fig. 10 are typical for all basin simulations but, in the simulations with 2-km-high mountains, the mixed layer in the basin stays below mountain height. The decrease in the mixed-layer height over the plains near the mountain base is an interesting feature that has not been simulated in previous numerical studies of a similar type. In a numerical study by Lu and Turco (1994), for example, thermally driven wind systems were simulated for a single mountain ridge, but the mixed-layer height does not decrease near the mountain ridge (cf. their Fig. 9). The study by Kimura and Kuwagata (1993) did not show this feature either. An observational study by de Wekker (1995) showed relatively low mixed-layer heights near a mountain base, but it is not entirely clear yet what physical processes played a role in those observations. For the sake of clarity, when we refer to the mixed layer over the plains in this study, we mean the mixed layer over the plains close to the mountain base.

Vertical profiles of potential temperature frequently show a ''two-layer'' temperature structure in the basin. Above a shallow well-mixed layer in the basin, a layer is present that decreases in stability during the day and eventually merges with the shallow mixed layer to form a deep mixed layer in the afternoon. This two-layer temperature structure as produced by the model is similar to observations in different valleys and basins (Whiteman 1982; Kondo et al. 1989; Kuwagata and Kimura 1995).

In all primary simulations, the mixed layer over the plains grows either well above mountain height (0.5- and 1-km height mountains) or to a height that is approximately equal to the mountain height (2-km height mountains). In almost all these simulations, a plain-to-basin wind occurs except for a few simulations with a very wide basin. According to Kimura and Kuwagata (1993), a plain-to-basin wind should fail to occur if the mixed-layer height over the plains is lower than the mountain height. To examine whether this is true, a simulation was carried out in which the initial temperature profile was modified at heights lower than 2300 m MSL, so that an inversion of 10 K was present between 2000 and 2300 m MSL. In this way, the mixed layer over the plains grew only to about 1 km AGL the following day, well below a 2-km height mountain. Surprisingly, even in this situation a plain-to-basin wind with a comparable magnitude develops where the upslope wind on the plainside slope transports air from the plains to the basin atmosphere. Thus, it appears that the mixed-layer height over the plains does not necessarily have to be larger than mountain height to generate a plain-to-basin flow. There is some evidence from observations in the vicinity of the Front Range in Colorado that supports this numerical result. A regional-scale wind system similar to the plain-to-basin wind, transporting air from the region east of the Front Range to the intermountainous region to the west (King 1996; Bossert and Cotton 1994) occurred sometimes when the mixed-layer height over the plains was lower than the average ridge-top height (White and King 1997).

The relationship between the late afternoon mixed-layer height over the plains and the occurrence or nonoccurence of the plain-to-basin wind is shown schematically in Fig. 11. The diagram depicts four cases of potential temperature fields prior to the possible onset of a plain-to-basin wind, as based on numerical simulations. In cases 1 and 2, the mixed-layer height over the plains is well below mountain height and the mixed-layer temperature in the basin boundary layer is warmer than over the plains. Case 1 is similar to the situation that Kimura and Kuwagata (1993) describe where no plain-to-basin winds develop. In this situation no large-scale temperature gradient exists above mountain height between the basin and the plains atmosphere. Case 2, with a mixed-layer height over the plain as in case 1, is similar to the aforementioned simulation where a plain-to-basin wind does develop. Cases 2 and 3 both

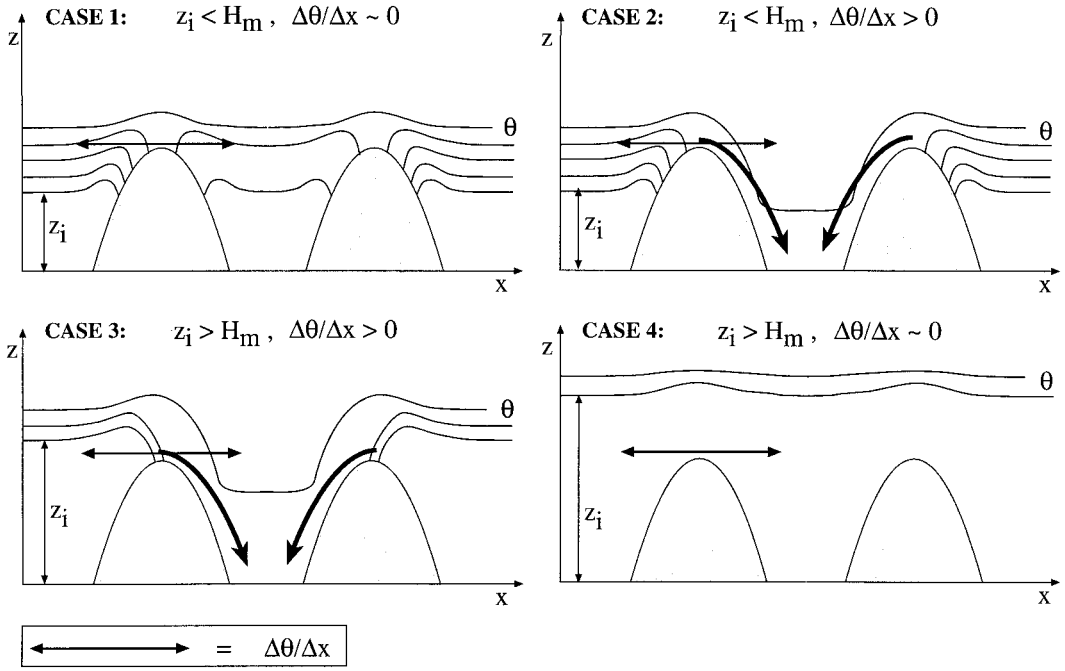

FIG. 11. A schematic diagram depicting four cases of late afternoon potential temperature fields based on model simulations. The cases differ in the horizontal temperature gradient above mountain height as evaluated over the distance indicated by the horizontal line, and the mixed-layer height over the plains z_i relative to mountain height H_m. The arrows directed into the basin in cases 2 and 3 indicate the development of a plain-to-basin wind around or after sunset.

show a horizontal temperature gradient above mountain height between the basin and plains, while the height of the mixed layer over the plains differs. In case 3, the mixed layer over the plains is higher than the mountain, a situation that is generally encountered in our simulations. In all those situations, a plain-to-basin wind develops except for a few with a very wide basin. In case 4, horizontal temperature gradients are very small and mixed-layer heights are similar everywhere. This case is best approximated by some of the 0.5-km height mountain simulations with wide basins where plain-to-basin winds do not develop. However, the mixed-layer height tends follow the orography in all the simulations in this study and was not as level as might be inferred in case 4.

The four cases described above indicate that plain-to-basin winds develop only if a horizontal temperature gradient is present above mountain ridge height with warmer air over the basin topography such that a hydrostatically established pressure gradient is directed toward the basin atmosphere. To demonstrate the importance of the horizontal temperature gradient above the mountain ridge, the strength of the plain-to-basin wind was investigated as a function of this horizontal temperature gradient. To separate the plain-to-basin wind from the locally generated downslope flows, several simulations were carried out with a single mountain ridge so that no basin was present. Subsequently, differences in the u component of the wind between this single mountain ridge simulation and basin simulation were determined for the east-facing slope. The maximum difference that occurred between 1800 and 2300 LST at heights below 500 m above the basinside slope was then defined as ''the net plain-to-basin wind'' Δu. Note that if the difference was zero, no plain-to-basin wind would be present. In Fig. 12a, Δu is plotted against $\Delta\theta/\Delta x$ for basins whose floors are at the same elevation as the plain ($\alpha = 0$). The horizontal temperature gradient was evaluated at 1900 LST at 100 m above the mountain height over the width of the mountain, as depicted by the figure at the top of Fig. 12a. It is clear that the maximum plain-to-basin flow strength increases roughly linearly with this horizontal temperature gradient. The outlier that is present for the 0.5-km mountain height is caused by the relatively early start (just before 1900 LST) of the plain-to-basin wind in that case and the resulting earlier decrease of the horizontal temperature gradient. The two cases with the largest basin widths had negligible horizontal temperature gradients.

In the case of basin topographies with an elevated basin floor, additional simulations were carried out in which again the mountain ridge on the east side of the basin was removed. The height of the surface to the east of the single mountain ridge was now taken to be equal to the basin floor height. Winds for this single mountain simulation were then compared to the winds from the elevated basin simulations. Figure 12b shows the results for elevated and nonelevated basins for the 1-km height mountain simulations. As before, Δu increases with $\Delta\theta/\Delta x$. For more elevated basins, Δu be-

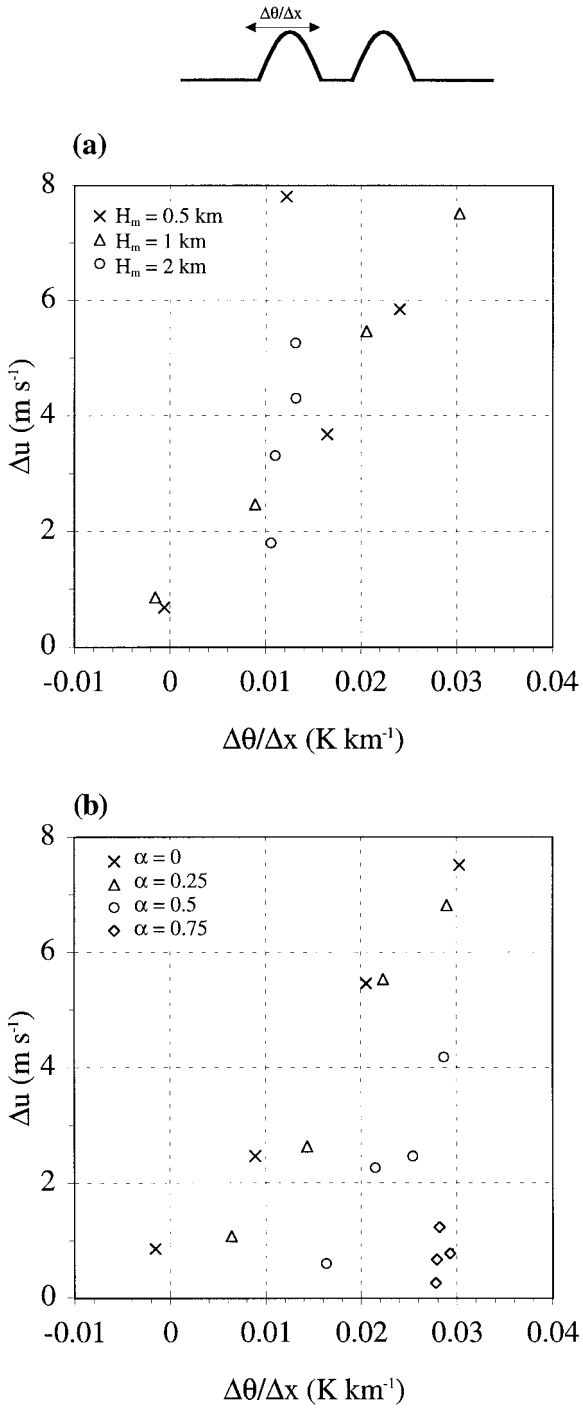

FIG. 12. Net plain-to-basin wind Δu as a function of the horizontal temperature gradient above mountain height $\Delta\theta/\Delta x$ for (a) different mountain heights and (b) different basin floor heights. Here, Δu was obtained by subtracting the wind field over the east-facing slope in the single mountain-ridge simulation from the wind field over the east-facing basinside slope and taking the maximum difference between 1800 and 2300 LST. Here, $\Delta\theta/\Delta x$ was evaluated at 1900 LST at the location indicated in the figure at the top of the plot.

comes smaller although $\Delta\theta/\Delta x$ increases. In those cases, it is the elevated heat source effect that is mainly responsible for the establishment of a horizontal temperature gradient above mountain height. The effect of the basin on this horizontal temperature gradient decreases as basin floor elevation increases.

To summarize, the horizontal temperature gradient above mountain height rather than the mixed-layer height over the plains relative to mountain height determines whether or not a plain-to-basin wind will occur. Only if an above-mountain horizontal temperature gradient exists with warmer air over the basin atmosphere than over the plain atmosphere can a plain-to-basin wind develop. As long as the differences in temperature between the basin and the plains are confined below mountain height, no plain-to-basin wind will occur.

To identify the key processes that determine the heating above the mountain height, a heat budget analysis was carried out. Since the numerical model produces a thermodynamically balanced dataset, the heating rate should equal the sum of the horizontal and vertical potential temperature advection, the turbulent heat flux divergence, and the radiative flux divergence. The magnitude of the daytime average of each of these terms as a function of horizontal distance is shown in Fig. 13 for a 20-km-wide basin with (a) $H_m = 0.5$ km, $\alpha = 0$; (b) $H_m = 1$ km, $\alpha = 0$; and (c) $H_m = 1$ km, $\alpha = 0.5$. The heat budget terms were averaged over a 500-m-thick layer above the mountain ridges, as depicted in the figure at the top of Fig. 13. Total heating rates are largest over the basin topography for each of these terrain configurations so that horizontal temperature gradients are created, eventually producing a plain-to-basin wind. Focusing on the basin center and the plains, it can be seen that for the 0.5-km height mountain (Fig. 13a), the turbulent flux divergence contributes the most to the total heating, while for the 1-km height mountain (Fig. 13b), vertical advection (i.e., subsidence) plays the most important role. Since the mixed layer over the basin center and the plains stays below mountain height during most of the day for the 1-km-deep basin simulation (see Fig. 10), heating due to turbulent flux divergence above mountain height is negligible. It is evident that subsidence heating may play a very important role in the creation of a horizontal temperature gradient. This explains why in case 2 in Fig. 11, a plain-to-basin wind develops even though the mixed layer over the basin center and plains stays well below mountain height. For the elevated basin (Fig. 13c), the layer in which the heat budget terms are evaluated is well mixed during most of the day and heating due to turbulent heat flux divergence is more important, which is similar to the 0.5-km height mountain (Fig. 13a). Nevertheless, the total heating rate over the basin center for the elevated basin (Fig. 13c) is only marginally larger than for the nonelevated basin with the same mountain height (Fig. 13b), indicating the importance of subsidence heating in that

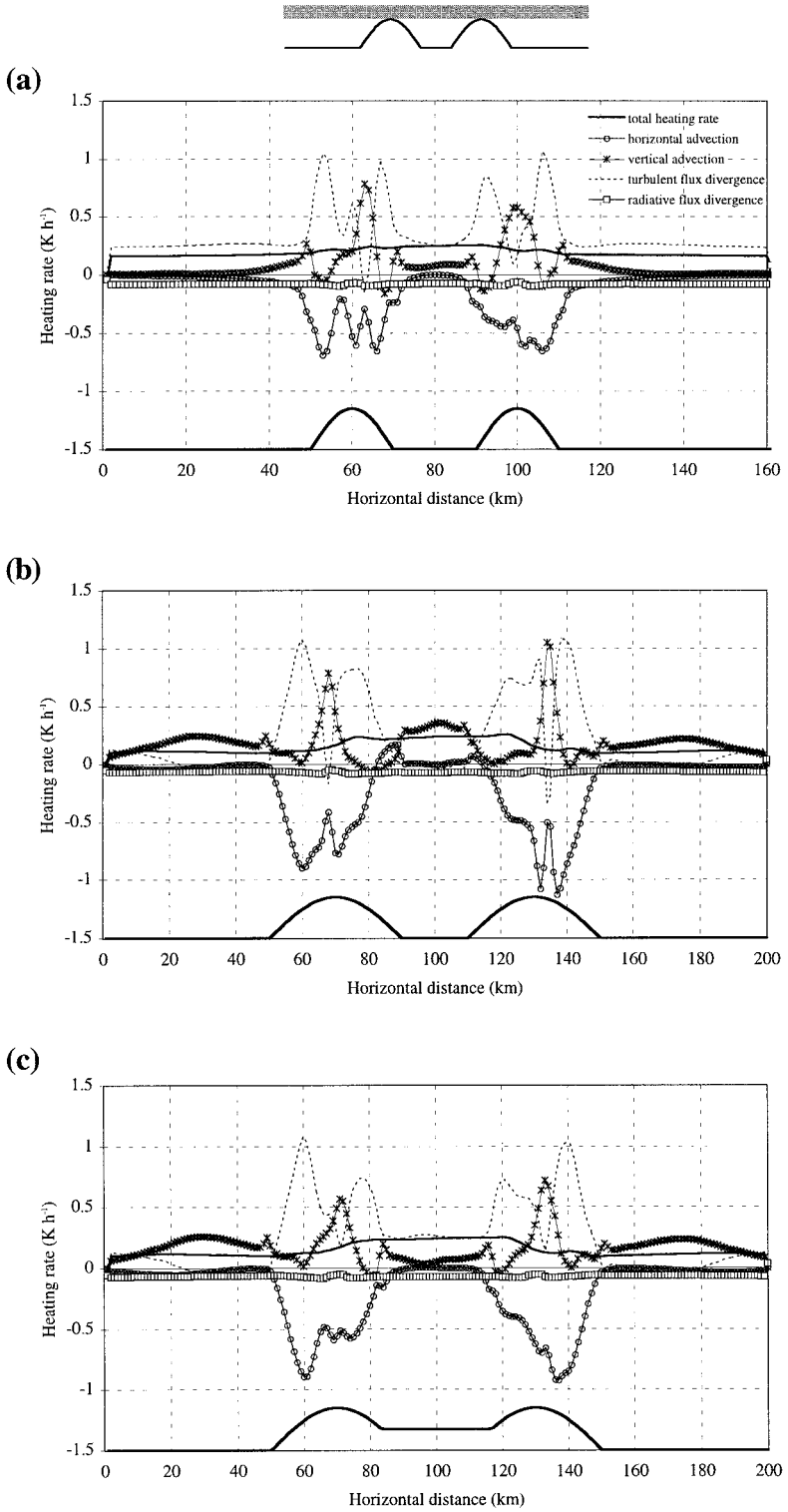

FIG. 13. Daytime-averaged values of the individual terms in the heat budget equation as a function of horizontal distance for basin topographies with (a) $H_m = 0.5$ km, $W_b = 20$ km, $\alpha = 0$; (b) $H_m = 1$ km, $W_b = 20$ km, $\alpha = 0$; and (c) $H_m = 1$ km, $W_b = 20$ km, $\alpha = 0.5$. The terms are vertically averaged over a 500-m-thick layer, as depicted in the figure at the top of the figure.

case. The contribution of radiative flux divergence is small in all three simulations.

In the 500-m-thick layer, turbulent flux divergence contributes most to the heating over the mountain slopes due to proximity to the elevated surface and the larger turbulent sensible heat fluxes over the mountain slopes, as discussed in section 3. Because of cold air advection by the upslope winds, however, the total heating rate is not larger over the mountain slopes than over the basin center.

6. Discussion

It was shown in section 3 that the model predicts a larger diurnal temperature range in the basin atmosphere than over the plains atmosphere and that larger sensible heat fluxes over the sidewalls combined with the volume effect account for this. The larger turbulent heat exchange on sloping surfaces than on flat surfaces, despite identical surface properties, is an important feature of the numerical simulations in this study. Unfortunately, observations are not available to support these model results. A few studies have shown an increase of turbulent sensible heat flux on sloping terrain (Mannstein 1988; Whiteman et al. 1989), but these were attributed largely to the different surface properties over the sloping terrain, not to higher turbulent heat exchange caused by the presence of slope winds. Future investigations should clarify whether the numerical model is overpredicting turbulent sensible heat fluxes over sloping terrain and whether these enhanced fluxes play an important role in establishing the larger diurnal temperature range in actual basins and valleys. Overpredicting the turbulent heat exchange over sloping terrain would have major consequences for the simulation of processes in the mountain boundary layer, including the overprediction of thermally induced flows and incorrect prediction of mixed-layer heights. Therefore, future observational research of surface–atmosphere exchange processes over mountainous terrain is highly desirable.

Factors such as inhomogeneous soil properties and the ambient wind might affect the plain-to-basin wind. Previous studies have indicated that inhomogeneous surface properties, in particular soil moisture, have an important effect on the simulation of thermally driven wind systems in mountainous terrain (Ookouchi et al. 1984; Benjamin 1986). Plain–basin differences in the surface sensible heat flux due to different surface properties can enhance or weaken the heating rate in basins or valleys relative to that over the plains. Those inhomogeneities may affect the strength and depth of slope flows, mixed-layer height, vertical motions and thus the horizontal temperature gradient above mountain height between the basin and the plains. For example, for a higher soil moisture on the basin floor and sidewalls than over the plains, the horizontal temperature gradient above mountain height can be expected to be smaller, resulting in a weaker plain-to-basin wind.

The ambient wind is also expected to influence the plain-to-basin wind. Several simulations were carried out in which the ambient wind speed was increased. Imposing a light westerly wind speed of only 1 m s^{-1} had a significant effect on the timing and strength of the plain-to-basin wind. For the western mountain ridge, the plain-to-basin wind starts 2 h earlier than in the case of a 0.1 m s^{-1} ambient wind. The maximum plain-to-basin flow is about 1 m s^{-1} stronger, although the timing of this maximum is very similar to the 0.1 m s^{-1} ambient wind case. On the eastern mountain ridge, ambient winds that are larger than 1 m s^{-1} completely suppress the plain-to-basin wind.

Factors related to numerical modeling of atmospheric processes, particularly initialization time, also affect the simulation of the plain-to-basin wind. To investigate the effect of model initialization time on the plain-to-basin wind simulations, several simulations were initialized with a 0500 LST (instead of 1700 LST) July 1988 average Grand Junction temperature sounding. Because model initial conditions are horizontally homogeneous, the simulation with the morning initialization starts off with an equal temperature structure in the basin and over the plains, while the simulation with the evening initialization develops a much colder basin atmosphere by morning. Consequently, temperature differences between plain and basin atmospheres in the afternoon are larger with the morning initialization. Therefore, the simulations initialized in the morning show stronger plain-to-basin winds for the same basin topography. Initializing in the evening, as was done in this study, is more justifiable since observations show much colder temperatures in the basin than over the plains in the morning hours (Maki et al. 1986; Kondo et al. 1989).

7. Summary and conclusions

A series of two-dimensional numerical experiments with idealized basin topographies was carried out to investigate the diurnal temperature range in a basin and the thermally driven plain-to-basin wind. Characteristics of the plain-to-basin wind were described and the mechanisms that affect its development were discussed.

The model predicts a larger diurnal temperature range in the basin atmosphere than over the plains atmosphere. The larger diurnal temperature range is primarily produced by much larger nighttime minimum temperatures than daytime maximum temperatures as compared to the minimum and maximum temperatures over the plains atmosphere. Previous investigators have explained the larger diurnal temperature range in basin–valley atmospheres as compared to the atmosphere over the plains to a volume effect, which can quantitatively be expressed in terms of a topographic amplification factor (TAF). Indeed, an increase in TAF is accompanied by an increase in diurnal temperature range in our model simulations. However, this diurnal temperature range increase is not due to the volume effect alone but

is due, in large degree, to the larger simulated turbulent sensible heat flux on the sloping terrain compared to that over flat terrain. This effect combines with the volume effect to give an almost linear relationship between TAF and the basin–plain diurnal temperature range ratio but with much higher values of this ratio than would be expected from consideration of the volume effect alone.

Simulations show that, in the morning, the upslope wind on the basinside slope starts 1–2 h earlier than over the plainside slope. Consequently, the upslope wind convergence zone is located on the plainside slope initially and shifts toward the basinside slope during the course of the day as the air in the basin becomes warmer than over the plains. Eventually, the plain-to-basin wind develops around or just after sunset when horizontal pressure gradients between the plains and the basin become large enough to overcome the upslope wind that is present on the basinside slope. A plain-to-basin wind developed in almost all simulations except for some of the simulations with the widest basins where symmetric circulations developed on both sides of the ridges. The maximum strength of the plain-to-basin wind increases with larger mountain height and narrower basin floor width, while basin floor elevation had no significant effect on the maximum strength. The timing of the plain-to-basin wind maximum did not vary significantly between the different basin topographies.

An analysis of mixed-layer heights revealed that in the morning hours and early afternoon the boundary layer growth is significantly reduced in the basin and in the plains regions that are adjacent to the mountain bases. Based on a previous numerical study of the plain-to-basin wind, the mixed-layer height was thought to be an important factor in determining the occurrence of the plain-to-basin wind with no plain-to-basin winds occurring when the mixed-layer height over the plains is lower than the mountain height. In almost all simulations, the mixed layer over the plains grows up to or above the mountain height and a plain-to-basin wind is generated. But a simulation where the mixed-layer height over the plains stayed well below mountain height still showed the presence of a plain-to-basin wind.

Model simulations show that the existence of a horizontal temperature gradient above mountain height is a necessary condition for the development of the plain-to-basin wind. As long as this gradient is present, a plain-to-basin wind can develop. Although the ratio of the mixed-layer height over the plains to the mountain height may affect the plain-to-basin wind by modifying the horizontal temperature gradient above mountain height, this ratio is not a critical factor for its development. Even if the mixed-layer height over the plains is lower than the mountain height, air can still be transported from the plains to the basin atmosphere.

The processes that generate an above-mountain horizontal temperature gradient were investigated by analyzing the individual terms in the heat budget equation, and it was concluded that both subsidence and turbulent heat flux divergence are important processes above the basin. The relative importance of subsidence and turbulent heat flux divergence depends on the mixed-layer height relative to the mountain height. If the mixed-layer height is higher than the mountain height, turbulent divergence dominates. With mixed-layer heights that do not exceed the mountain height, the relatively strong subsidence over the basin can still establish an above-mountain horizontal temperature gradient and a plain-to-basin wind can still occur. For elevated basins, the basin floor acts like an elevated heat source, similar to plateaus, thus producing horizontal temperature gradients above mountain height by relatively large turbulent heat flux divergence.

The plain-to-basin flow may play an important role in the transport of air pollutants over complex terrain but has not been studied as extensively as other wind systems in complex terrain. Because of the interactions of multiscale circulations in actual topography, it will be difficult to observe a pure plain-to-basin wind. Therefore, comparisons of observations with numerical simulation are difficult to make. By carrying out a systematic set of idealized simulations, we have attempted to determine the factors that are important for the development of the plain-to-basin wind. From these simulations, it can be inferred that the plain-to-basin wind may be an important component in the observed complex flow patterns over basin topography.

Acknowledgments. This research was carried out while the first author was a visiting student at Pacific Northwest National Laboratory (PNNL) from Wageningen Agricultural University, the Netherlands. Associated Western Universities–Northwest division is acknowledged for arranging his stay at PNNL through their graduate research program. The authors thank Dr. Chris Doran and Meinolf Kossmann for their comments on the manuscript. This research was supported by the Environmental Sciences Division of the U.S. Department of Energy under Contract DE-AC06-76RLO 1830 at PNNL under the auspices of the Atmospheric Studies in Complex Terrain Program. PNNL is operated by Battelle Memorial Institute for the U.S. Department of Energy.

REFERENCES

Benjamin, S. G., 1986: Some effects of surface heating and topography on the regional severe storm environment. Part II: Two-dimensional idealized experiments. *Mon. Wea. Rev.,* **114,** 330–343.

Bossert, J. E., 1997: An investigation of flow regimes affecting the Mexico City region. *J. Appl. Meteor.,* **36,** 119–140.

——, and W. R. Cotton, 1994: Regional-scale flows in mountainous terrain. Part I: A numerical and observational comparison. *Mon. Wea. Rev.,* **122,** 1449–1471.

Burger, A., and E. Ekhart, 1937: Über die tägliche Zirkulation der Atmosphäre im Bereich der Alpen (On the diurnal circulation

of the atmosphere in the region of the Alps). *Gerlands Beitr. Geophys.*, **49,** 341–367.

Chen, C., and W. R. Cotton, 1983: A one-dimensional simulation of the stratocumulus-capped mixed layer. *Bound.-Layer Meteor.*, **25,** 289–321.

de Wekker, S. F. J., 1995: The behaviour of the convective boundary layer height over orographically complex terrain. M.S. thesis, Institute for Meteorology and Climate Research, University of Karlsruhe, Dept. of Meteorology, Wageningen Agricultural University, 74 pp.

Doran, J. C., and S. Zhong, 1994: Regional drainage flows in the Pacific Northwest. *Mon. Wea. Rev.*, **122,** 1158–1167.

Fast, J. D., 1995: Mesoscale modeling and four-dimensional data assimilation in areas of highly complex terrain. *J. Appl. Meteor.*, **34,** 2762–2782.

——, S. Zhong, and C. D. Whiteman, 1996: Boundary-layer evolution within a canyonland basin: Part II: Numerical simulations of nocturnal flows and heat budgets. *J. Appl. Meteor.,* **35,** 2162–2178.

Jackson, P. L., and D. G. Steyn, 1994: Gap winds in a fjord. Part I: Observations and numerical simulation. *Mon. Wea. Rev.*, **122,** 2645–2665.

Kimura, F., and T. Kuwagata, 1993: Thermally induced wind passing from plain to basin over a mountain range. *J. Appl. Meteor.*, **32,** 1538–1547.

King, C. W., 1996: A climatology of thermally forced circulations in oppositely oriented airsheds along the Continental Divide in Colorado. Ph.D. dissertation, University of Colorado, 199 pp.

Kleinschmidt, E., 1922: Der tägliche Gang des Windes in der freien Atmosphäre und auf Berggipfeln (The diurnal course of the wind in the free atmosphere and on mountain tops). *Beitr. Phys. Atmos.*, **10,** 1–15.

Klemp, J. B., and R. B. Wilhelmson, 1978a: The simulation of three-dimensional convective storm dynamics. *J. Atmos. Sci.,* **35,** 1070–1096.

——, and ——, 1978b: Simulations of right- and left-moving storms produced through storm splitting. *J. Atmos. Sci.*, **35,** 1097–1110.

Kondo, J., T. Kuwagata, and S. Haginoya, 1989: Heat budget analysis of nocturnal cooling and daytime heating in a basin. *J. Atmos. Sci.,* **46,** 2917–2933.

Kurita, H., H. Ueda, and S. Mitsumoto, 1990: Combination of local wind systems under light gradient wind conditions and its contribution to the long-range transport of air pollutants. *J. Appl. Meteor.,* **29,** 331–348.

Kuwagata, T., and F. Kimura, 1995: Daytime boundary layer evolution in a deep valley. Part I: Observations in the Ina Valley. *J. Appl. Meteor.,* **34,** 1082–1091.

Louis, J. F., 1979: A parametric model of vertical eddy fluxes in the atmosphere. *Bound.-Layer Meteor.,* **17,** 187–202.

Lu, R., and P. Turco, 1994: Air pollutant transport in a coastal environment. Part I: Two-dimensional simulations of sea-breeze and mountain effects. *J. Atmos. Sci.,* **51,** 2285–2308.

Mahrer, Y., and R. A. Pielke, 1977: A numerical study of the airflow over irregular terrain. *Beitr. Phys. Atmos.,* **50,** 98–113.

Maki, M., T. Harimaya, and K. Kikuchi, 1986: Heat budget studies on nocturnal cooling in a basin. *J. Meteor. Soc. Japan,* **64,** 727–740.

Mannouji, N., 1982: A numerical experiment on the mountain and valley winds. *J. Meteor. Soc. Japan,* **60,** 1085–1105.

Mannstein, H., 1988: The spatial variation of sensible heat flux in the Alps from satellite data. *Proc. of Eighth EARSeL Symp.*, Capri, Italy, 356–367.

McKee, T. B., and R. D. O'Neal, 1989: The role of valley geometry and energy budget in the formation of nocturnal valley winds. *J. Appl. Meteor.,* **28,** 445–456.

Ookouchi, Y., M. Segal, R. C. Kessler, and R. A. Pielke, 1984: Evaluation of soil moisture effects on the generation and modification of mesoscale circulations. *Mon. Wea. Rev.,* **112,** 2281–2292.

Pielke, R. A., and Coauthors, 1992: A comprehensive meteorological modeling system—RAMS. *Meteor. Atmos. Phys.,* **49,** 69–91.

Reiter, E. R., and M. Tang, 1984: Plateau effects on diurnal circulation patterns. *Mon. Wea. Rev.,* **112,** 638–651.

Staley, D. O., 1959: Some observations of surface-wind oscillations in a heated basin. *J. Meteor.,* **16,** 364–370.

Steinacker, R., 1984: Area–height distribution of a valley and its relation to the valley wind. *Contrib. Atmos. Phys.,* **57,** 64–71.

Toth, J. J., and R. H. Johnson, 1985: Summer surface flow characteristics over northeast Colorado. *Mon. Wea. Rev.,* **113,** 1458–1469.

Tyson, P. D., and R. A. Preston-Whyte, 1972: Observations of regional topographically induced wind systems in Natal. *J. Appl. Meteor.,* **11,** 643–650.

Wagner, A., 1932: Der tägliche Luftdruck- und Temperaturgang in der freien Atmosphäre und in Gebirgstälern (The diurnal course of pressure and temperature in the free atmosphere and in mountain valleys). *Gerlands Beitr. Geophys.,* **37,** 315–344.

——, 1938: Theorie und Beobachtung der periodischen Gebirgswinde (Theory and observation of periodic mountain winds). *Gerlands Beitr. Geophys.,* **52,** 408–449.

White, A. B., and C. W. King, 1997: A comparison of mixing depths observed over horizontally inhomogeneous terrain. *EURASAP Workshop on Determination of Mixing Height,* Roskilde, Denmark, 123–126.

Whiteman, C. D., 1982: Breakup of temperature inversions in deep mountain valleys: Part I: Observations. *J. Appl. Meteor.,* **21,** 270–289.

——, 1990: Observations of thermally developed wind systems in mountainous terrain. *Atmospheric Processes Over Complex Terrain, Meteor. Monogr.,* No. 45, Amer. Meteor. Soc., 5–42.

——, K. J. Allwine, L. J. Fritschen, M. M. Orgill, and J. R. Simpson, 1989: Deep valley radiation and surface energy budget microclimates. Part II: Energy budget. *J. Appl. Meteor.,* **28,** 427–437.